

AV₃Sb₅ kagome superconductors: a review with transport measurements

Zhuokai Xu,^{1,2} Tian Le,^{1,2} and Xiao Lin^{1,2,*}

¹Key Laboratory for Quantum Materials of Zhejiang Province, Department of Physics,
School of Science and Research Center for Industries of the Future,
Westlake University, Hangzhou 310030, P. R. China

²Institute of Natural Sciences, Westlake Institute for Advanced Study, Hangzhou 310024, P. R. China
(Dated: February 21, 2025)

Kagome systems have garnered considerable attention due to the unique features of the sublattice structure and band topology. The recently discovered kagome metals AV₃Sb₅ (where A = K, Rb, Cs) host a rich array of symmetry-breaking phases, including exotic charge density waves (CDW), electronic nematicity, pair density waves (PDW) and superconductivity. Despite extensive experimental and theoretical investigations into the diverse phases, several key issues remain contentious, such as a solid clarification of the time-reversal symmetry breaking (TRS-breaking) in the CDW order and its implications for the nature of superconducting (SC) pairing symmetry. This review aims to shed light on the transport properties of these intertwined phases, emphasizing the pivotal role that transport measurements play in uncovering the non-trivial quantum states of matter.

1. Introduction. Introduced by Syozi in 1951¹, the kagome lattice is composed of corner-sharing triangles that form a hexagonal structure. Each triangle contains three sublattices per unit cell, marked by different colors in Fig. 1a. This structure is geometrically frustrated. Given the nearest-neighbor antiferromagnetic exchange interaction, the kagome lattice, with its geometric spin frustration, serves an ideal platform for exploring quantum spin liquid². A standard tight-binding model on the kagome lattice yields a nontrivial electronic band structure, featuring two van Hove singularities at M -point for electron filling of $f = 5/12$ and $3/12$, a Dirac point at K -point for $f = 1/3$ and a flat band³⁻⁵, as seen in Fig 1b. Consequently, by adjusting the electron filling, the kagome lattice exhibit a variety of emergent phases of matter, shaped by the combined effect of topology and strong correlations⁶. Once the filling approaches the van Hove singularity, the kagome model, incorporating on-site repulsion (U) and nearest-neighbor interaction (V_1), produces an exceptionally rich phase diagram, including charge bond-density wave^{4,5}, spin density wave^{3,4}, pair-density wave⁷, Z2 Chern insulator⁸ as well as unconventional superconductivity^{3-5,9}.

In 2019, Ortiz et al. reported the discovery of vanadium-based kagome metals, AV₃Sb₅ (A = K, Rb, Cs)¹⁰. These compounds are layered materials, crystallizing in the P6/mmm space group. As illustrated in Fig. 1c. V-atoms constitute the kagome skeleton, with the V-Sb block responsible for the distinctive physical properties, while the alkali metal atoms serve as spacers between the layers. Later on, superconductivity was identified with the critical temperature, $T_c \approx 3$ K for CsV₃Sb₅¹¹ and 0.9 K for KV₃Sb₅¹² and RbV₃Sb₅¹³. Before entering the SC phase as temperature (T) lowers, AV₃Sb₅ undergoes a first-order CDW phase transition^{11,14-17}, which is highly nontrivial¹⁸⁻²² and may

represent the long-sought chiral flux phase^{23,24}. Additionally, a reduction in rotational symmetry from C6 to C2 was observed within the CDW phase²⁵, likely signaling the presence of electronic nematicity^{26,27}. As T further lowers below T_c , a PDW phase emerges^{28,29}, where the SC pairing amplitude modulates periodically in real space. These complex symmetry-breaking phases, either competing or intertwining with each other, is reminiscent of that observed in the high- T_c cuprates.

In the past few years, transport measurements have become an essential tool for probing the complex quantum phases of AV₃Sb₅. This review aims to emphasize their pivotal role and is organized as follows: we begin with an introduction to the basic electronic properties of AV₃Sb₅, drawing insights from quantum oscillation (QO) measurements. Next, we delve into the transport signatures of the CDW phase and the associated emergent symmetry breaking. Third, we present the current understanding of the SC order, highlighting nontrivial features such as time-reversal symmetry breaking (TRS-breaking), as unveiled by quantum transport techniques. Finally, we conclude with an outlook, addressing unresolved questions and suggesting potential future directions in the study of Kagome superconductors. This review may not cover all aspects of Kagome systems; for a broader understanding, one may refer to other insightful reviews³⁰⁻³⁵.

2. Basic electronic properties. The electronic band structure of AV₃Sb₅ retains key features of the ideal kagome model, but exhibits greater complexity^{11,12,36-41}. Density functional theory (DFT) calculations reveal multiple bands near the Fermi level (E_F)^{11,37}, as shown in Fig. 1d for CsV₃Sb₅. An electron-like parabolic band emerges around the Γ point, stemming from the Sb p_z -orbital. At the Brillouin zone (BZ) boundaries, the band structure is dominated by V $3d$ -orbitals. Dirac points are at the zone corner K . And several van Hove singularities (vHSs) are observed at the the zone edge M , with two located close to E_F . The Fermi surface nesting at these vHSs, com-

* linxiao@westlake.edu.cn

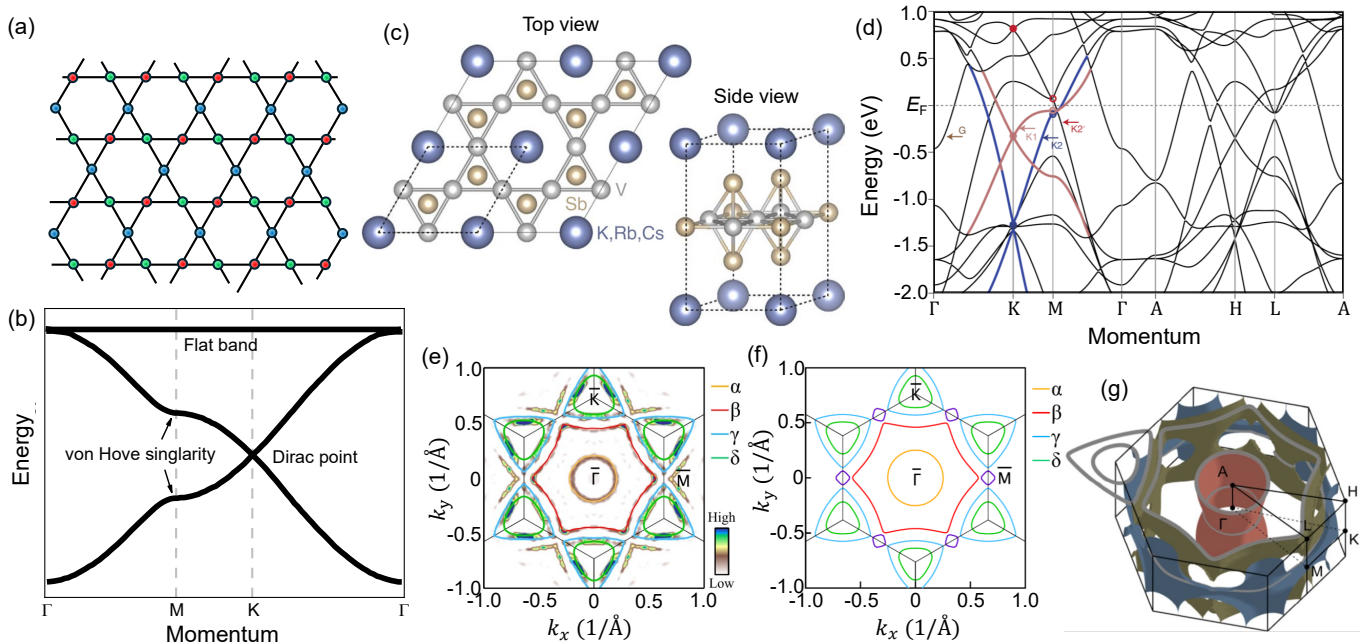


FIG. 1. (a) Kagome Lattice. The three sublattices are marked by different colors. (b) Band structure of kagome lattice from the nearest-neighbor tight-binding model. (c) Crystal structure of AV_3Sb_5 ¹⁷. (d) Calculated band structure of CsV_3Sb_5 ¹⁷, showing four bands (G , $K1$, $K2$ and $K2'$) crossing Fermi level. vHSs at M and Dirac points at K stems from $K1$, $K2$ and $K2'$ kagome bands and are marked by open and solid circles, respectively. (e) Fermi surface mapping of KV_3Sb_5 from ARPES measurements³⁶. (f) Calculated Fermi surface at $k_z = \pi/c$ for undistorted KV_3Sb_5 ³⁶. (g) 3D Fermi surface for undistorted CsV_3Sb_5 ³⁷. Here, (c) and (d) are taken from Ref. 17; (e) and (f) are taken from Ref. 36; (g) is taken from Ref. 37.

combined with the divergence in the density of states (DOS), is believed to play a pivotal role in enabling pairing across multiple channels³⁻⁵. AV_3Sb_5 also exhibits a non-trivial Z_2 topological index¹¹. Angle-resolved photoemission spectroscopy (ARPES) have identified the corresponding topological surface state, embedded around the bulk Fermi surface at M point³⁹.

Fig. 1e-g present a comparative study of experimental and calculated band dispersions and Fermi surfaces for AV_3Sb_5 ^{17,37}. The Fermi pocket demonstrates a quasi-2D nature, indicating weak interlayer interactions between neighboring V-Sb blocks³⁷. The close agreement between ARPES and DFT calculations suggests only minor band renormalization, underscoring the weak correlation effects (small U) in the material⁴². Additionally, high resolution ARPES measurements have detected Fermi surface distortion induced by the CDW phase^{36,40,41}. Kang *et al.* observed an unusual energy splitting in the vHS and Dirac bands, which is attributed to band folding in reconstructed BZ and points to a specific nature of the CDW phase (see more discussion below)¹⁷.

The multiple Fermi pockets in AV_3Sb_5 have intensively been investigated using QO measurements^{33,37,43-47}. When subjected to strong magnetic field (B), the electronic bands are quantized into discrete Landau levels. As B increases, the Landau levels are progressively squeezed out of Fermi level, resulting in periodical oscillation in physical quantities associated with Fermi surface. The QO period/frequency is indicative of the size

of Fermi surface, specifically representing the extreme cross-section of Fermi pockets normal to B (Onsager relation). Additionally, the T -dependence of QO amplitude can be utilized to extract the effective electron mass (m^*) through the Lifshitz-Kosevich theory. QO measurements are particularly powerful for detecting small Fermi pockets owing to the high energy resolution (sub-meV)⁴⁸, making it a crucial complement in the study of solid-state band structures. The primary techniques of QOs include the quantum Hall effect, Shubnikov-de Haas (SdH) effect (magnetoresistance)^{37,44,45}, and de Haas-van Alphen (dHvA) effect (magnetization)⁴⁶. Besides that, QOs can be observed in phenomena such as the Seebeck effect³³, Nernst effect³³, thermal Hall effect⁴⁷ and tunnel diode oscillator (TDO)⁴³.

For CsV_3Sb_5 , QO measurements have unveiled complex oscillation patterns. Fourier transform allows the resolution of up to 25 frequencies (F)⁴³. They are categorized into three regimes. In the low- F regime (less than 250 T), four peaks of 18, 26, 73, and 92 T have been identified in various reports^{37,45}, as seen in Fig 2a,b. The estimated m^* for these bands are relatively small, approximately one-tenth of the free electron mass. The peak of 73 T is consistently reported and attributed to a small Fermi pocket near the L (\bar{M}) point of the unfolded BZ^{43,44} in Fig 1f. However, the other three F are not well-resolved by ARPES and DFT calculations, necessitating further investigation. In the mid- F regime (250 < F < 2500 T), a dozen of F have been identi-

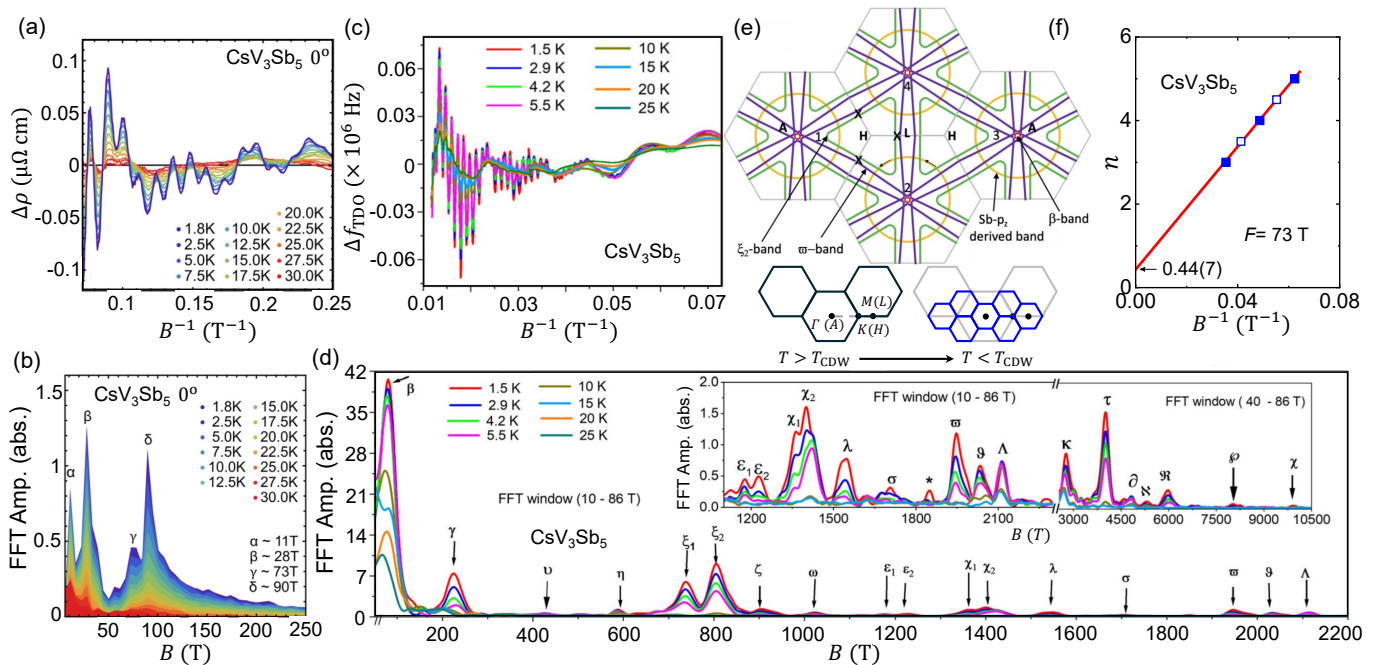


FIG. 2. (a) QOs of magnetoresistance measured up to 14 T for CsV_3Sb_5 ³⁷. (b) Fourier transformation of the QO data in a, showing four frequency peaks below 250 T. (c) QOs of TDO frequency measured up to 86 T for CsV_3Sb_5 ⁴³. (d) Fourier transformation of the QO data in (c), showing multiple frequencies up to 10 kT. (e) Upper: Schematic of the 2×2 folded Fermi surface of CsV_3Sb_5 $k_z = \pi/c$ owing to CDW distortion⁴³. Lower: Evolution of BZs across the CDW distortion. (f) Landau fan diagram for the frequency of 73 T, revealing a nontrivial band topology⁴⁴. Here, (a-b) are taken from Ref. 37; (c-e) are taken from Ref. 43; (f) are taken from Ref. 44.

fied seen in Fig. 2c,d, though the exact number varies across different reports^{37,43,46}. This variation is due to differences in sample quality, the maximum of applied field and the resolution of QO techniques among different researches. F in this regime is believed to account for the major Fermi pockets of CsV_3Sb_5 . For instance, two F around 736 and 804 T arise from the bands derived from Dirac crossings at the K and H points, respectively (see the triangles in Fig 2e)⁴³. In the high- F regime (> 2500 T), a few peaks have been identified, reaching up to 10 kT⁴³, as shown in the inset of Fig 2d. The estimated size of the corresponding Fermi surface is comparable to or even exceeds that of the folded first BZ in the CDW state. Chapai *et al.* attributed this observation to magnetic breakdown⁴³, a phenomenon arising from quantum tunneling of quasiparticles across closely spaced Fermi surfaces in the k -space.

The dimensionality of Fermi surface can be explored by angle dependent QO measurements. For a 3D isotropic Fermi surface, F is angle independent. While in 2D case, F follows $F(\theta) = F(0^\circ)/\cos\theta$, where θ is the angle of B . In CsV_3Sb_5 , the presence of both quasi-2D and 3D Fermi pockets at different F has been demonstrated by previous studies^{44,46}. It reflects subtle features of the band structure induced by the specific organization of the CDW state. In addition to the frequency and amplitude, the phase (ϕ) of QO also plays a pivotal role in uncovering non-trivial band topology. ϕ is expressed as: $\phi = 2\pi(\frac{F}{B} + \frac{1}{2} - \frac{\Phi_B}{2\pi} + \delta)$, where Φ_B represents

the Berry phase and δ is a dimensionality factor with $\delta = 0$ for 2D and $\delta = \pm\frac{1}{8}$ for 3D Fermi surface. In Fig. 2f, the Landau fan diagram for CsV_3Sb_5 reveals non-trivial Berry phase ($\Phi_B = \pi$) at $F \approx 73$ T, underscoring the topological character of the corresponding band^{43,44}. This serves an important indication of topologically non-trivial band structure, a feature frequently discussed in kagome systems. Note that KV_3Sb_5 and RbV_3Sb_5 also exhibit rich QO spectra that bear recognizable similarity to CsV_3Sb_5 ^{13,50}. However, there is a slight difference in F , which may reflect subtle variations in the nature of CDW distortion in the three materials.

3. CDW order. The CDW develops below $T_{\text{CDW}} \approx 78, 104$ and 94 K in AV_3Sb_5 with $A = \text{K, Rb}$ and Cs , respectively. In Fig. 3a, an anomaly in T -dependent resistivity (ρ) marks the CDW transition for CsV_3Sb_5 . It corresponds to the sharp peak observed in heat capacity in Fig. 3b, implying a first-order transition¹¹. The CDW modulation of local DOS has been extensively mapped using surface-sensitive scanning tunneling microscopy (STM) techniques^{14,15,21,22}, as exemplified in Fig 3c. Fourier transform, presented in Fig. 3d, reveals six additional ordering peaks, indicating a 3Q CDW order with a 2×2 superlattice modulation. This modulation corresponds to a breathing mode of kagome lattice showing either the Star of David (SoD) or trihexagonal (TrH) distortions⁵¹, depicted in Fig 3e. The TrH phase is predicted to be more energetically favorable⁵¹.

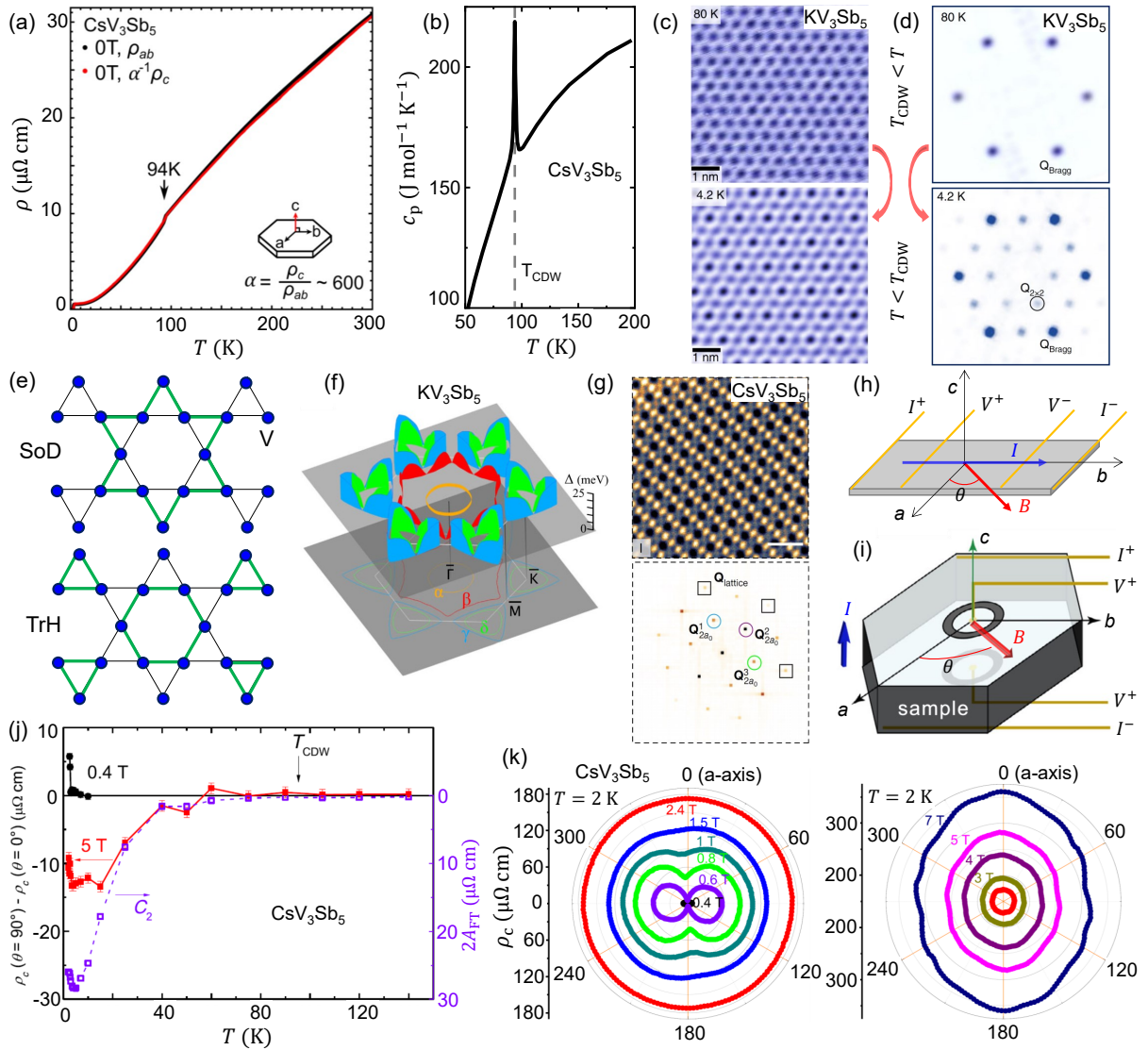


FIG. 3. (a) Temperature dependence of resistivity within in-plane and along c -axis for CsV_3Sb_5 ¹¹. The anomaly at 94 K corresponds to the CDW transition. (b) Temperature dependence of heat capacity¹¹, showing a sharp peak at $T_{\text{CDW}} \approx 94$ K for CsV_3Sb_5 . (c) STM topographic image on the Sb surface of KV_3Sb_5 above T_{CDW} (upper) and below T_{CDW} (down). Below T_{CDW} , the surface shows a 2×2 modulation. (d) Fourier transform of the Sb topographic image above T_{CDW} (upper) and below T_{CDW} (down)²¹. The Fourier transform shows only Bragg peaks ($\mathbf{Q}_{\text{Bragg}}$) at $T > T_{\text{CDW}}$ and additional order peaks ($\mathbf{Q}_{2 \times 2}$) appears at $T < T_{\text{CDW}}$. (e) Schematic of SoD and TrH distortion within the Kagome layer in the CDW order. (f) Momentum-dependent CDW gaps at the Fermi surface for KV_3Sb_5 ³⁶. (g) Nematic phase revealed by STM topography and the corresponding Fourier transform in CsV_3Sb_5 ²⁶. (h) Setup for angle-dependent resistivity measurement with the field and current applied within the ab -plane. (i) Corbino-shaped setup for angle-dependent c -axis resistivity measurement⁴⁹. (j) Temperature dependence of C_2 symmetry for CsV_3Sb_5 . The solid symbols denote the resistivity difference measured at 0.4 and 5 T and the open symbols denote the amplitude of C_2 peak from Fourier transform. (k) Polar plot for angle-dependent c -axis resistivity below 2.4 T (left) at $T < T_c$, showing two-fold symmetry, and above 2.4 T (right), with the two-fold pattern rotated by 90° . Here, (a-b) are taken from Ref. 11; (c-d) are taken from Ref. 21; (f) is taken from Ref. 36; (g) is taken from Ref. 26; (i-k) are taken from Ref. 49.

Moreover, STM indicates a CDW gap of approximately 50 meV^{14,15,21,52}, which is strongly anisotropic over the V-derived Fermi surfaces, as evidenced by ARPES in Fig. 3f³⁶.

The mechanisms underlying the CDW state are complicated. In Fig. 3f, the anisotropic CDW gap shows a pronounced maximum around the M point³⁶, implying

the significance of inter-saddle-point scattering channels between different vHSs⁴¹. This point was supported by other ARPES measurements^{17,53} as well as several studies employing optical spectroscopy⁵⁴. Moreover, hard X-ray scattering experiments on $(\text{Cs,Rb})\text{V}_3\text{Sb}_5$ did not detect acoustic phonon anomalies, indicative of weak electron-phonon coupling⁵⁵. Taken together, these re-

sults suggest the dominant role of Fermi surface nesting in driving the CDW transition. In stark contrast, other investigations, including Raman scattering⁵⁶, neutron scattering⁵⁷, and optical conductivity⁵⁸ measurements, observed strong electron-phonon coupling in AV_3Sb_5 , emphasizing its importance in the development of the CDW state. Evidence for this coupling is also seen in a kink in the energy dispersion observed in ARPES measurements of KV_3Sb_5 ³⁶. DFT calculations revealed soft phonon modes at both M and L points of the BZ, and their condensation is proposed to facilitate the formation of the CDW^{51,59}. Furthermore, a combination of ARPES and DFT studies in CsTi_3Bi_5 , a Ti-based kagome system analogous to AV_3Sb_5 , reported that the presence of van Hove singularities alone is insufficient to drive the CDW transition⁶⁰. It appears that both the Fermi surface nesting and electron-phonon coupling are essential for the CDW order.

According to DFT calculations⁵¹, phonon softening at L point leads to a structural modulation along the c-axis in AV_3Sb_5 . The 3D CDW order in this kagome family has been reported in various studies^{15,37,55,59}, with slight discrepancies among its members. High-resolution X-ray diffraction (XRD) measurements revealed a $2 \times 2 \times 2$ lattice distortion in KV_3Sb_5 and RbV_3Sb_5 ^{55,61}, characterized by a staggered trihexagonal (TrH) arrangement, i.e. a π phase shift between neighboring kagome layers¹⁷. For CsV_3Sb_5 , both $2 \times 2 \times 2$ and $2 \times 2 \times 4$ distortions were observed to coexist^{37,61,62}, and one study reported a transition from the $2 \times 2 \times 4$ to the $2 \times 2 \times 2$ order as T decreases below 60 K⁶³. The complex 3D CDW states in CsV_3Sb_5 are thought to result from a stacking of kagome sheets exhibiting alternating SoD and TrH distortions^{17,61}. It appears that the different orders in AV_3Sb_5 are close in energy and highly sensitive to external perturbations such as disorder and frozen strains^{61,62}.

Rotational symmetry breaking. Besides translation symmetry breaking, rotational symmetry breaking from C6 to C2 has been extensively documented in the CDW phase. Previous STM study revealed lattice modulation along one of the three crystallographic directions, resulting in an imbalance among the amplitude of three CDW vectors (\mathbf{Q}_{2a_0})²⁶, as seen in Fig. 3g. This C2 symmetry appears at the Fermi level and is linked to the electronic nematic phase. This transition occurs at $T_{\text{nem}} \approx 35$ K according to the measurements of nuclear magnetic resonance (NMR) and elastoresistance²⁶. Unidirectional electronic scattering of coherent quasiparticles was also detected by STM below 30 K²⁷. Additionally, a $4a_0$ stripe order was observed by some STM studies in CsV_3Sb_5 (at $T^* \approx 60$ K)^{14,27} and RbV_3Sb_5 ²², but not in KV_3Sb_5 ^{21,25}. This order is thought to be a surface state, as it is not resolved by bulk-sensitive techniques like NMR and XRD.

The rotational symmetry breaking can be effectively resolved by angle-dependent magnetoresistance (AMR) measurements^{49,64}. An early in-plane AMR study detected a twofold anisotropy, whose orientation rotates

by 60° upon entry into the SC phase⁶⁴. In this setup, with the current (I) and B applied within the ab-plane (seen in Fig. 3h), orbital effects induced by Lorentz force generally lead to artificial C2 symmetry. Subsequently, Xiang *et al.* measured angle-dependent c-axis resistivity (ρ_c) by using a Corbino-shaped electrode configuration, as illustrated in Fig. 3i, wherein B rotates within the plane, always normal to I ⁴⁹. This measurement revealed a twofold rotational symmetry below 40 – 60 K, persisting into the SC state as shown in Fig. 3j,k. In the SC phase, the field direction, corresponding to the minimum resistance, is aligned with one of the crystalline axes, suggesting a maximum in the SC gap, as seen in Fig. 3k. When a stronger field was applied to disrupt superconductivity, the twofold pattern rotated by 90°, highlighting the nematicity in the normal state. Furthermore, recent calorimetry measurements showed a twofold anisotropy superimposed on a sixfold background in the in-plane upper critical field, indicating a nematic SC order parameter⁶⁵.

Elastoresistivity measurements are an effective tool for probing nematic phase transitions. Elastoresistivity, a fourth-rank symmetric tensor, quantifies the change in resistivity under external strain, expressed as

$$m_{ij} = \frac{\partial(\Delta\rho/\rho)_i}{\partial\varepsilon_j} \quad (1)$$

where ε_j represents the strain tensor, and $\Delta\rho$ denotes the resistivity change induced by strain. The indices $i, j = 1 - 6$ follow Voigt notation with $1 = xx$, $2 = yy$, $3 = zz$, $4 = yz$, $5 = zx$ and $6 = xy$. Elastoresistivity coefficients can be grouped into different symmetry channels according to the irreducible representations (irrep) of the lattice point group. For the Kagome system with D_{6h} symmetry, the coefficient of the isotropic A_{1g} irrep defined as $m_{A_{1g}} = m_{11} + m_{12} + m_{13}[2\nu_{ac}/(1 - \nu_{ab})]$ with ν_{ac} and ν_{ab} the Poisson ratio. For the anisotropic E_{2g} irrep, the coefficient is $m_{E_{2g}} = m_{11} - m_{12}$. The measurement of elastoresistivity generally employs three methods: the differential elastoresistivity technique, the modified Montgomery technique, and the transverse technique⁶⁶, as illustrated in Fig. 4a.

In the context of nematic phase transitions, nematic susceptibility, linked to $m_{E_{2g}}$, is expected to diverge as T approaches T_{nem} . In Fig. 4b, the T -dependence of $m_{E_{2g}}$, measured by differential techniques, shows a sharp jump at T_{CDW} and continues to rise down to $T_{\text{nem}} \approx 35$ K for CsV_3Sb_5 ²⁶. This phenomenon is distinct from the Curie-Weiss trend typically observed in a continuous nematic phase transition. The authors attributed it to nematic fluctuations pinned by the pre-existing C2 structural distortion in the 3D CDW phase. A subsequent work reported optimized superconductivity in the vicinity of a nematic quantum critical point in Ti-doped CsV_3Sb_5 ⁶⁷.

Conversely, Liu *et al.* carried out a more systematic study of the elastoresistivity using all three techniques and observed a distinct behavior in Fig. 4c-e⁶⁶. Specif-

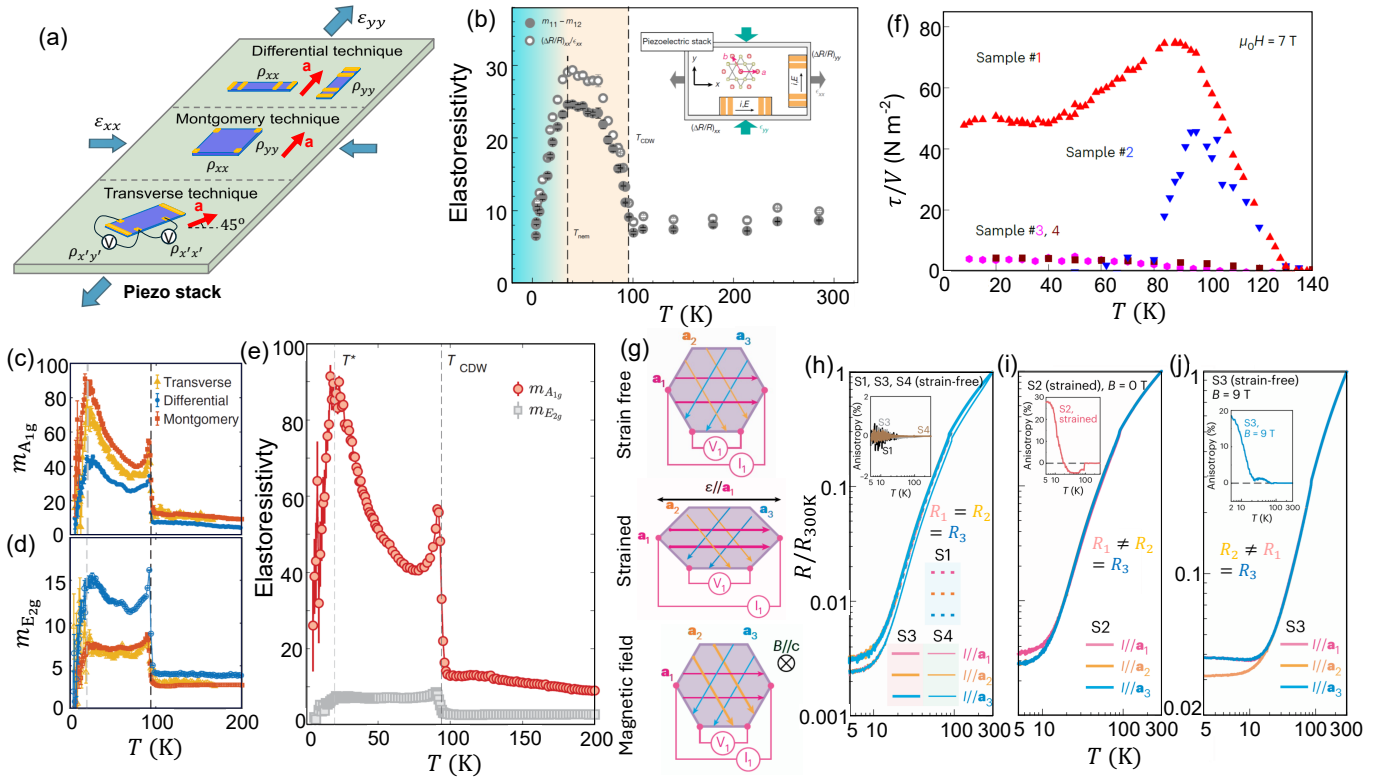


FIG. 4. (a) Schematic of three setups for elasto-resistivity measurements: the differential technique, Montgomery technique and transverse technique. (b) Temperature dependence of elasto-resistivity coefficients ($m_{E_{2g}}$) for CsV_3Sb_5 measured using the differential technique²⁶. (c-d) Temperature dependence of elasto-resistivity coefficients in the isotropic A_{1g} and anisotropic E_{2g} channels for CsV_3Sb_5 , measured with all three techniques, respectively⁶⁶. (e) Comparison of $m_{A_{1g}}$ and $m_{E_{2g}}$ from the data in (c-d), obtained using the Montgomery technique. (f) Temperature dependence of magnetic torque normalized by the sample volume for different samples of CsV_3Sb_5 ⁶⁸. (g) Schematic illustration of in-plane electric transport under different conditions: strain free, in-plane strain and perpendicular external field. The resistance is measured along the three main axes. (h-j) Temperature dependence of tri-directional resistance for CsV_3Sb_5 under conditions of strain-free (h), strain (i) and magnetic field (j)⁶⁹. Here, (b) is taken from Ref. 26; (c-e) are taken from Ref. 66; (f) is taken from Ref. 68; (g-j) are taken from Ref. 69.

ically, $m_{A_{1g}}$, rather than $m_{E_{2g}}$, show a prompt jump at T_{CDW} , followed by a continuous increase as T decreases to 20 K in Fig. 4e. In contrast, $m_{E_{2g}}$ shows a slight jump but remains flat both below and above T_{CDW} . The authors suggested that the pronounced $m_{E_{2g}}$ signal in previous reports arises from cross-contamination from the A_{1g} channel, a common problem in differential techniques. Their findings indicate the absence of nematic phase transition within the CDW phase in CsV_3Sb_5 . Similar observations were reported in Ref. 70. Several reports proposed that the C2 symmetry arises from the interlayer coupling, i.e. a π -phase shift in the stacking of adjacent SoD or TrH distorted kagome layers^{15,26,49,70-72}.

In this context, recent magnetic torque (τ) measurements uncovered a two-fold in-plane magnetic anisotropy with an onset temperature of around 130 K, notably above T_{CDW} , as shown in Fig. 4f⁶⁸. The hysteretic behavior in τ under a conically rotated magnetic field provides thermodynamic evidence supporting the emergence of an odd-parity nematic order, a phenomenon that cannot be detected by an even-parity probe such as elasto-resistivity. However, other bulk thermodynamic probes, such

as elastocaloric effect⁶⁶ and thermal expansion⁷⁰, didn't observe any anomaly above T_{CDW} .

A unified understanding of the C2 symmetry and nematicity in kagome superconductors remains an important target. Guo *et al.* reported the absence of anisotropy in strain-free CsV_3Sb_5 samples over the full temperature range, seen in Fig. 4g-j⁶⁹. However, once either a weak perpendicular field or in-plane strain are present, a pronounced in-plane transport anisotropy appears below T_{CDW} in Fig. 4h-j. While both perturbations yield similar anisotropic behavior, their underlying mechanisms differ: strain directly breaks rotational symmetry, whereas the field is proposed to stabilize the flux order coexisting with bond order⁶⁹. This stark contrast in origin highlights the system's sensitivity to external perturbations, which may offer some insights to the controversy surrounding the entangled CDW orders.

Time reversal symmetry breaking. The most outstanding feature of the CDW order in AV_3Sb_5 is TRS-breaking. Although the absence of long-range magnetic ordering is confirmed by neutron scattering experiments⁷³, zero-field

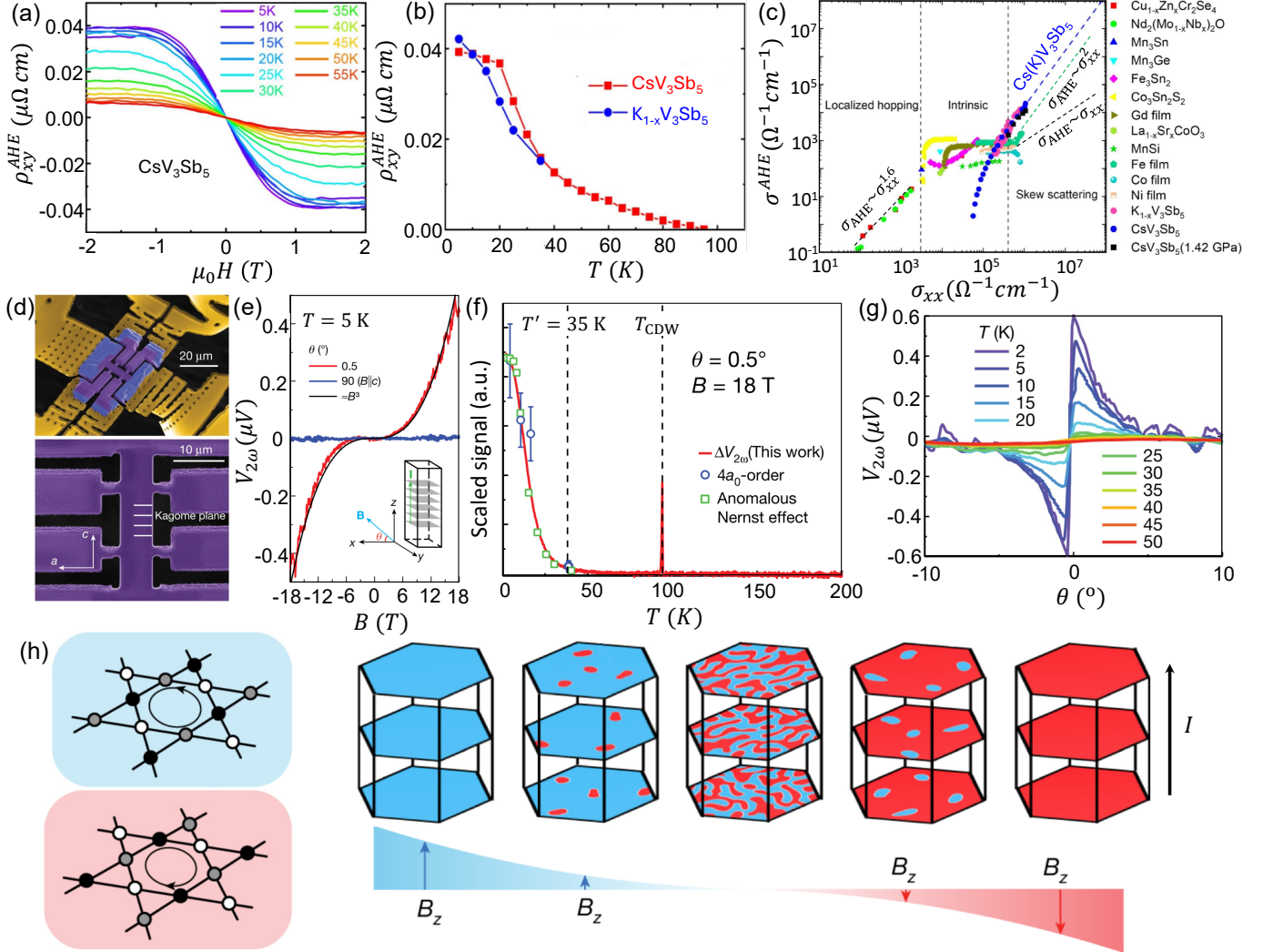


FIG. 5. (a) Anomalous Hall resistivity (ρ_{xy}^{AHE}) measured at various T below T_{CDW} in CsV_3Sb_5 ⁴⁵. (b) Temperature dependence of ρ_{xy}^{AHE} for CsV_3Sb_5 and KV_3Sb_5 , showing an increase below T_{CDW} ⁴⁵. (c) Scaling of anomalous Hall conductivity (σ^{AHE}) with electric conductivity (σ_{xx}) for multiple materials including CsV_3Sb_5 ⁴⁵. (d) Low-strain device fabricated by focused ion beam, with current applied along the c -axis. (e) Field dependence of second harmonic voltage ($V_{2\omega}$) with current applied along the c -axis. (f) Temperature dependence of $V_{2\omega}$, compared with signals from other probes. $V_{2\omega}$ shows a peak at $T = T_{\text{CDW}}$ and significantly increases at $T < 35$ K. (g) Angular dependence of $V_{2\omega}$ at $B = 18$ T and various temperatures. (h) Schematic illustration of chiral charge order domains with chirality controlled by the out-of-plane field component¹⁹. Here, (a-c) are taken from Ref. 45; (d-h) are taken from Ref. 19.

μSR measurements detected an apparent increase of the internal field below T_{CDW} , which persists into the SC phase, suggesting the presence of unconventional TRS-breaking charge orders¹⁸. TRS-breaking signals were also observed through magneto-optical Kerr effect and circular dichroism measurements, with the onset coinciding with the CDW transition²⁰. Simultaneously, scanning birefringence measurements revealed three C2 domains, approximately $100 \mu\text{m}$ in size, oriented at $2\pi/3$ angles with respect to each other²⁰. From the STM measurements, the intensity peaks of charge modulation in the Fourier transform show chiral anisotropy, the chirality of which can be reversed by applying an external mag-

netic field in the opposite direction^{21,22}. Moreover, recent studies revealed the chirality of CDW peaks modulated by linearly polarized light along high-symmetry directions⁷⁴. This optically switchable chirality, combined with field tunability, suggests a peculiar piezo-magnetic effect. Such behavior strongly indicates TRS-breaking, potentially arising from orbital magnetization inherent to the CDW phase.

Transport measurements are an importance probe for detecting TRS-breaking phases. A giant anomalous Hall (AHE) effect has been reported in AV_3Sb_5 with its onset temperature concurrent with T_{CDW} ^{45,75}, as shown in Fig. 5a-b. The scaling of σ_{AHE} and σ_{xx} for AV_3Sb_5 is pre-

sented in Fig. 5c⁷⁵, in comparison with other systems. The scaling relationship differs across different regimes as σ_{xx} increases. In the localized hopping regime, a side-jump effect causes σ_{AHE} to follow a $\sigma_{xx}^{1.6}$ dependence. In the intrinsic regime, the AHE is generated by the Berry curvature, making σ_{AHE} independent of σ_{xx} . Finally, in the pure regime, skew scattering dominates and σ_{AHE} becomes linear in σ_{xx} . In Fig. 5c, σ_{AHE} of AV_3Sb_5 follows a quadratic scaling, similar to that of iron in the skew scattering regime, but with a much larger skew constant. While the exact mechanism for the giant AHE in AV_3Sb_5 is yet to be resolved, it is thought to be closely tied to the enhanced skew scattering in the CDW state and the large Berry curvature arising from the kagome lattice^{45,75}. Besides AHE, the exotic feature could also be manifested in anomalous effects in thermal and thermoelectric transports^{33,47}. It is important to note that the AHE in AV_3Sb_5 does not exhibit a typical hysteresis behavior as that of ferromagnetic ordering, therefore it is not a definitive proof of TRS-breaking.

Using focused ion beams, Guo *et al.* fabricated strain-relaxed CsV_3Sb_5 devices with the current applied along the *c*-axis and reported field-switchable nonlinear transports, as seen in Fig. 5d-e. For B applied at small θ with respect to the *ab*-plane, they observed second harmonic voltage generation ($V_{2\omega}$) at low temperatures, closely linked to the transitions within the CDW state, as shown in Fig. 5f. This phenomenon could be interpreted by the electronic magnetochiral anisotropy (eMChA), which requires orthogonal orientations of the electric current \mathbf{I} , magnetic field \mathbf{B} and the direction of inversion symmetry breaking. In Fig. 5g, $V_{2\omega}$ is zero at $\theta = 0^\circ$ ($\mathbf{B} \parallel$ *ab*-plane) and increases rapidly as θ deviates from zero. It peaks at $\theta \approx 0.5^\circ$, before diminishing at larger θ (larger out-of-plane component of field B_z). Moreover, the polarity of $V_{2\omega}$ is reversed as θ evolves from positive to negative by inverting B_z . Such a field-switching polarity suggests the TRS-breaking charge order.

The microscopic origin of the observed second harmonic generation remains unclear. The authors proposed a phenomenological model involving chiral charge order domains, as illustrated in Fig. 5h. The chiral domain structure is by nature spatially asymmetric, disrupting in-plane mirror symmetry and can be tuned by B_z . For small θ , B_z induces an imbalance in domains of opposite chirality, leading to strong chiral scattering at domain walls and resulting in large eMChA. As B_z increases at larger θ , the domains become fully polarized. In this case, the intrinsic chiral scattering process within the domains is too weak to produce observable eMChA. At $\theta = 0^\circ$, domains of opposite chirality are in equilibrium. Therefore, the global transport measurements observed averaged signals with vanishing eMChA. In this context, B_z adjusts domain chirality, while the in-plane component (B_{in}) ensures orthogonality, enabling finite eMChA.

Theoretically, the TRS-breaking charge order in AV_3Sb_5 is likely a chiral flux phase, a long-sought order first proposed for the honeycomb lattice in Hal-

dane's model⁷⁶ and later for the square lattice of cuprates by Varma⁷⁷. In the Kagome lattice, the chiral flux phase with orbital current is energetically favorable near the van Hove filling due to the unique sublattice structure^{23,78}. The imbalance of anti-clockwise triangle current flux loop and a clockwise hexagonal flux loop leads to a net signal of TRS-breaking. However, it should be noted that a definitive conclusion regarding the chiral flux phase in AV_3Sb_5 remains controversial. Other conflicting studies, including μSR ⁷⁹, STM^{16,25}, and polar optical Kerr effect⁸⁰ measurements, have failed to detect signals of TRS-breaking.

4. Superconducting orders. The superconductivity of the Kagome systems remains a critical topic of research, with ongoing debates on the pairing mechanism and pairing symmetry. The interplay between the complex CDW order and superconductivity^{85,86} leads to the PDW order^{28,29} and further complicates the understanding of the SC state, raising the fundamental question of whether it is conventional or unconventional.

From the experimental viewpoint, thermal conductivity measurements in CsV_3Sb_5 revealed a residual linear term in κ at zero- T ⁸⁷, which is often associated with nodal superconductivity. Similar results were observed in KV_3Sb_5 and RbV_3Sb_5 through μSR , where the SC penetration depth (λ) exhibited a linear temperature dependence⁸⁸. In contrast, in CsV_3Sb_5 , λ measured by μSR ⁸⁹ and TDO⁹⁰ followed an exponential temperature dependence, suggesting a fully gapped superconductivity. STM studies yielded conflicting results: both V-shaped (nodal gap) and U-shaped (nodeless gap) scanning tunneling spectroscopy (STS) profiles were observed in CsV_3Sb_5 , suggesting the complexity of the gap structure^{28,52}.

Moreover, nuclear quadrupole resonance (NQR) measurements of the 121/123 Sb atoms showed a Hebel-Slichter coherence peak at T_c of CsV_3Sb_5 , which is widely regarded as a hallmark for conventional *s*-wave superconductivity⁹¹. Additionally, T_c in CsV_3Sb_5 is weakly sensitive to non-magnetic impurities introduced by electron irradiation, another indication of fully gapped pairing symmetry. By increasing the amount of impurities, λ , measured by TDO, reveals a gradual evolution from a highly anisotropic fully gapped SC state to an isotropic fully gapped state⁹². Recent high-resolution ARPES measurements examined the SC gap in momentum space and revealed multiple gaps with a highly anisotropic gap structure (80% anisotropy) at the hexagonal Fermi surface near the Brillouin zone boundary and isotropic gaps at other regions⁹³. Similar to this observation, STM studies unveiled residual in-gap states within the SC gaps and the corresponding Fermi arcs in *k*-space. These features might be related to the specific orbital structure of the PDW order²⁹. The multiple, anisotropic, fully-gapped, spin-singlet pair symmetry could help to reconcile the aforementioned conflicting observations.

On the other hand, first-principles calculations suggest that the electron-phonon coupling is too weak to

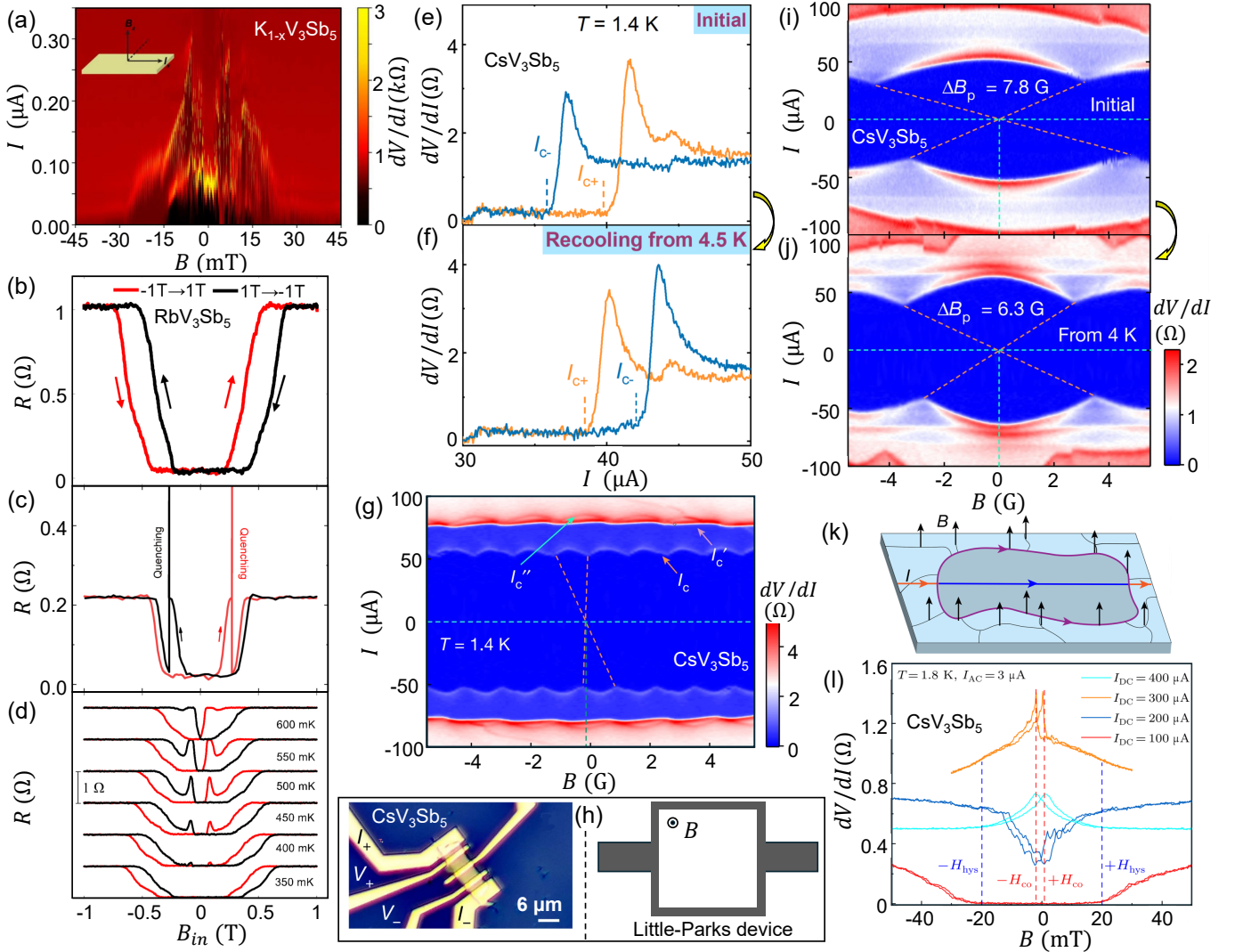


FIG. 6. (a) Color plots of dV/dI versus current and out-of-plane field for $K_{1-x}V_3Sb_5$ -based Josephson junctions measured at 20 mK⁸¹. (b-d) Field hysteresis of magnetoresistance for RbV_3Sb_5 measured in the SC state by applying in-plane field⁸². (e-f) Zero-field SDEs for CsV_3Sb_5 with its polarity modulated by thermal cycling. (g) Color plots of dV/dI versus current and out-of-plane field for CsV_3Sb_5 , where the critical current shows periodic oscillations. (h) Photo image of exfoliated CsV_3Sb_5 devices, compared with the configuration of a standard Little-Parks device. (i-j) Thermal modulation of oscillation patterns, showing variations in oscillation period. (k) Sketch of domain network, composed of chiral SC domains.⁸³ (l) Field hysteresis of dV/dI in the SC mixed state for CsV_3Sb_5 measured with out-of-plane field⁸⁴. Here, (a) is taken from Ref. 81; (b-d) are taken from Ref. 82; (g-k) are taken from Ref. 83; (l) is taken from Ref. 84.

account for the high T_c in AV_3Sb_5 , pointing to the possibility of unconventional pairing⁵¹. However, it is also proposed that the on-site correlations may be weak, disfavor unconventional superconductivity. Instead, non-local electron correlations, such as nearest-neighbor and next-nearest-neighbor interactions, are thought to play a crucial role in these materials. Several theoretical studies incorporating both on-site U and nearest-neighbor V_1 have predicted a rich phase diagram, spanning both conventional (s -wave) and unconventional (chiral $d \pm id$ or f -wave) superconductivity^{3-5,9}.

In AV_3Sb_5 , superconductivity develops within the pre-existing CDW states. The mutual evolution between

these two orders tuned by hydrostatic pressure or chemical doping has been widely reported in different studies, with CsV_3Sb_5 displaying an abnormal double-dome SC phase diagram^{35,85,86}. It indicates a complicated competition between the SC and CDW orders. Moreover, the ratio between T_c and $\lambda_{\text{eff}}^{-2}$ is significantly higher than that in conventional superconductors, indicative of a dilute superfluid density^{18,88,89}. These characteristics collectively suggest unconventionality in the SC phase.

Another question is whether the SC phase, intervening with the TRS-breaking charge order, disrupts TRS. While given the pre-existence of TRS-breaking in the normal state, zero- B μ SR failed to detect an additional

transition in the muon relaxation rate at T_c ¹⁸. Subsequent experiments observed a slight upturn in the muon relaxation rate across T_c , when the charge order is completely suppressed in AV_3Sb_5 ^{88,94}, which might be a signature of TRS-breaking superconductivity. Furthermore, Deng *et al.* reported B -tunable chirality of PDW intensity peaks in STM, pointing to the chiral PDW nature in AV_3Sb_5 ²⁹. When the CDW order is suppressed by Ta doping in $Cs(V_{1-x}Ta_x)_3Sb_5$, the same group observed a time-reversal asymmetric interference of Bogoliubov quasiparticles via external B inversion, supporting TRS-breaking superconductivity, in agreement with μ SR data⁹⁴.

Transport measurements have played a vital role in elucidating the pairing symmetry in AV_3Sb_5 . Fitting λ , estimated from the self-field critical current (I_c), suggests conventional s -wave superconductivity with strong coupling in CsV_3Sb_5 ⁹⁵. However, Josephson junctions based on non-SC $K_{1-x}V_3Sb_5$ show anomalous patterns in Fig 6a, including a minimum near zero B , which was interpreted by a possible spin-triplet pairing⁸¹. More recently, Wang *et al.* reported an unusual “advanced” hysteresis of the magnetoresistance in the SC state of RbV_3Sb_5 , as presented in Fig. 6b⁸². The hysteresis is pronounced upon sweeping in-plane B_{in} , but diminishes significantly and eventually disappears when B is tilted away from the ab -plane. The finite-resistance state within the hysteresis loop appears metastable and can be quenched to zero resistance after applying large I (heating process), as seen in Fig. 6c. Additionally, the magneto-resistance exhibits reentrant superconductivity upon sweeping B_{in} , as illustrated in Fig. 6d. To explain these observations, the authors proposed a TRS-breaking spin-triplet p -wave pairing state, hosting net spin-magnetic moments. TRS-breaking SC domains, composed of reversed spin-polarized pairing orders, interact with B_{in} , giving rise to the observed phenomena. However, this interpretation does not clarify why the effects are exclusively influenced by B_{in} . The proposed spin-triplet pairing contrasts sharply with prior reports⁸⁹⁻⁹³.

SC diode effects (SDEs) arise in systems lacking both TRS and inversion symmetry, manifesting as asymmetry in I_c with respect to the direction of current flow. Recently, SDEs have emerged as a novel tool for probing exotic SC orders in quantum materials. Le *et al.* reported the observation of SDEs in CsV_3Sb_5 flakes under zero B in Fig. 6e, which unveils internal TRS-breaking⁸³. The SDE polarity could be modulated by thermal cycling from T slightly above T_c as seen in Fig. 6f, potentially indicating a dynamic domain structure associated with the SC order. Furthermore, the authors observed double-slit interference patterns (DSIP) in I_c upon applying a small external B , as shown in Fig. 6g. These patterns resemble those seen in Little-Parks effects, which typically require a current loop with a hollow core, contrasting with the configuration of mechanically exfoliated CsV_3Sb_5 devices in Fig. 6h. The oscillation period, on the order of sev-

eral Gauss, corresponds to a flux-penetration area (loop size) of several μm^2 . The features of oscillations, such as the period and phase, also exhibit thermal modulation as seen in Fig. 6i,j. These phenomena are interpreted within a domain-network model, composed of TRS-breaking SC domains of opposite chirality, as illustrated in Fig. 6k. The evolution of chiral SC order parameter from one domain to its neighbors of opposite chirality leads to the suppression of the order parameter and generates boundary supercurrents flowing along the domain walls. This behavior mimics the supercurrent loop in a standard Little-Parks device, which is responsible for the observation of DSIP. The dynamics of SC domains can also be reflected by the observation of field hysteresis in the differential resistance within the mixed state, where vortices are depinned, seen in Fig. 6l⁸⁴. Taken together, the study of thermally modulated zero-field SDE and DSIP unveils dynamic TRS-breaking SC domains with edge supercurrents in CsV_3Sb_5 . This approach may serve as an effective tool to explore potential TRS-breaking superconductors.

5. Summary and outlook. The kagome AV_3Sb_5 system has emerged as one of the most rapidly advancing subjects in condensed matter physics since its discovery in 2019. A number of exotic and intervened orders have been observed, yet several fundamental questions lack comprehensive interpretation. In the normal state, the system exhibits a plethora of electronic orders that are nearly degenerate in energy and highly sensitive to external perturbations such as strain, magnetic field and polarized optical excitation. A solid demonstration of the long-sought chiral flux order remains a crucial goal in this field and demands the cooperation of multiple experimental techniques. Recent experimental studies suggest that the orbital magnetism manifests as a piezomagnetic effect^{69,74}, which warrants further exploration. It’s generally expected that the multiple orders would lead to complex domain structures in AV_3Sb_5 . C_2 symmetry domains have been observed by polarized MOKE measurements²⁰. While the detection of chiral domains with edge orbital current, an essential signature of chiral flux order, remains a big challenge. This will hopefully be solved by advanced field-sensitive scanning probes.

In AV_3Sb_5 , the SC order has converged to multiple, highly anisotropic, sign preserved, spin-singlet pair symmetry. When the CDW order is completely suppressed by chemical doping, an isotropic, fully gapped order parameter was resolved by ARPES, pointing to s -wave superconductivity⁹⁶. However, this conclusion disagrees with the observation of TRS-breaking signals in the SC state^{82-84,94}. A chiral $d + id$ state, combining nodeless superconductivity and broken TRS, may reconcile these conflicting observations. And the kagome sublattice symmetry potentially mitigates disorder-induced pairing breaking in spin-singlet d -wave states⁹⁷. A comprehensive understanding of the pairing symmetry will benefit from phase-sensitive techniques like Josephson junction experiments in the future. Moreover, Ge *et al.*

identified exotic charge- $4e$ and charge- $6e$ superconductivity in the fluctuating region of Cooper pair condensate in CsV_3Sb_5 ⁹⁸. Before drawing a firm conclusion, further studies are required to verify this unusual pairing, particularly direct detection of fractional flux quanta by spatially resolved probes such as STM and scanning SQUID.

Beyond the V-based Kagome system, novel AM_3X_5 variants, such as CsTi_3Bi_5 and CsCr_3Sb_5 , have recently been discovered to exhibit superconductivity and intriguing correlated orders^{99,100}. These systems offer new opportunities to explore unconventional electronic phenomena, extending the frontiers of kagome physics. A deeper understanding of the V-135 phase provides a foundation for unraveling the mechanisms underlying multiple electronic orders in these related materials. Hope this review has captured the rapid advancement in AV_3Sb_5 , offer-

ing insights into their complex interplay of charge ordering, superconductivity and other symmetry-breaking phenomena.

Acknowledgments. This research is supported by the National Key Research and Development Program of China under Grant No.2024YFA1408100 and National Natural Science Foundation of China under Grant No. 12474131. This research is supported by “Pioneer” and “Leading Goose” R&D Program of Zhejiang under Grant 2024SDX-HDX0007 and Zhejiang Provincial Natural Science Foundation of China for Distinguished Young Scholars under Grant No. LR23A040001. This research is supported by the Research Center for Industries of the Future (RCIF) at Westlake University under Award No. WU2023C009.

-
- [1] Syôzi I 1951 *Prog. Theor. Phys.* **6** 306
- [2] Balents L 2010 *Nature* **464** 199
- [3] Yu S L and Li J X 2012 *Phys. Rev. B* **85** 144402
- [4] Wang W S, Li Z Z, Xiang Y Y, and Wang Q H 2013 *Phys. Rev. B* **87** 115135
- [5] Kiesel M L, Platt C, and Thomale R 2013 *Phys. Rev. Lett.* **110** 126405
- [6] Kang M, Fang S, Ye L, Po H C, Denlinger J, Jozwiak C, Bostwick A, Rotenberg E, Kaxiras E, Checkelsky J G, and Comin R 2020 *Nat. Commun.* **11** 4004
- [7] Wu Y M, Thomale R, and Raghu S 2023 *Phys. Rev. B* **108** L081117
- [8] Guo H M and Franz M 2009 *Phys. Rev. B* **80** 113102
- [9] Wu X, Schwemmer T, Müller T, Consiglio A, Sangiovanni G, Di Sante D, Iqbal Y, Hanke W, Schnyder A P, Denner M M, Fischer M H, Neupert T, and Thomale R 2021 *Phys. Rev. Lett.* **127** 177001
- [10] Ortiz B R, Gomes L C, Morey J R, Winiarski M, Bordelon M, Mangum J S, Oswald I W H, Rodriguez-Rivera J A, Neilson J R, Wilson S D, Ertekin E, McQueen T M, and Toberer E S 2019 *Phys. Rev. Mater.* **3** 094407
- [11] Ortiz B R, Teicher S M L, Hu Y, Zuo J L, Sarte P M, Schueller E C, Abeykoon A M M, Krogstad M J, Rosenkranz S, Osborn R, Seshadri R, Balents L, He J, and Wilson S D 2020 *Phys. Rev. Lett.* **125** 247002
- [12] Ortiz B R, Sarte P M, Kenney E M, Graf M J, Teicher S M L, Seshadri R, and Wilson S D 2021 *Phys. Rev. Mater.* **5** 034801
- [13] Yin Q, Tu Z, Gong C, Fu Y, Yan S, and Lei H 2021 *Chin. Phys. Lett.* **38** 037403
- [14] Zhao H, Li H, Ortiz B R, Teicher S M, Park T, Ye M, Wang Z, Balents L, Wilson S D, and Zeljkovic I 2021 *Nature* **599** 216
- [15] Liang Z, Hou X, Zhang F, Ma W, Wu P, Zhang Z, Yu F, Ying J J, Jiang K, Shan L, Wang Z, and Chen X H 2021 *Phys. Rev. X* **11** 031026
- [16] Li H, Wan S, Li H, Li Q, Gu Q, Yang H, Li Y, Wang Z, Yao Y, and Wen H H 2022 *Phys. Rev. B* **105** 045102
- [17] Kang M, Fang S, Yoo J, Ortiz B R, Oey Y M, Choi J, Ryu S H, Kim J, Jozwiak C, Bostwick A, Rotenberg E, Kaxiras E, Checkelsky J G, Wilson S D, Park J H, and Comin R 2023 *Nat. Mater.* **22** 186
- [18] Mielke III C, Das D, Yin J X, Liu H, Gupta R, Jiang Y X, Medarde M, Wu X, Lei H C, Chang J, Dai P, Si Q, Miao H, Thomale R, Neupert T, Shi Y, Khasanov R, Hasan M Z, Luetkens H, and Guguchia Z 2022 *Nature* **602** 245
- [19] Guo C, Putzke C, Konyzheva S, Huang X, Gutierrez-Amigo M, Errea I, Chen D, Vergniory M G, Felser C, Fischer M H, Neupert T, and Moll P J W 2022 *Nature* **611** 461
- [20] Xu Y, Ni Z, Liu Y, Ortiz B R, Deng Q, Wilson S D, Yan B, Balents L, and Wu L 2022 *Nat. Phys.* **18** 1470
- [21] Jiang Y X, Yin J X, Denner M M, Shumiya N, Ortiz B R, Xu G, Guguchia Z, He J, Hossain M S, Liu X, Ruff J, Kautzsch L, Zhang S S, Chang G, Belopolski I, Zhang Q, Cochran T A, Multer D, Litskevich M, Cheng Z J, Yang X P, Wang Z, Thomale R, Neupert T, Wilson S D, and Hasan M Z 2021 *Nat. Mater.* **20** 1353
- [22] Shumiya N, Hossain M S, Yin J X, Jiang Y X, Ortiz B R, Liu H, Shi Y, Yin Q, Lei H, Zhang S S, Chang G, Zhang Q, Cochran T A, Multer D, Litskevich M, Cheng Z J, Yang X P, Guguchia Z, Wilson S D, and Hasan M Z 2021 *Phys. Rev. B* **104** 035131
- [23] Feng X, Jiang K, Wang Z, and Hu J 2021 *Sci. Bull.* **66** 1384
- [24] Park T, Ye M, and Balents L 2021 *Phys. Rev. B* **104** 035142
- [25] Li H, Zhao H, Ortiz B R, Park T, Ye M, Balents L, Wang Z, Wilson S D, and Zeljkovic I 2022 *Nat. Phys.* **18** 265
- [26] Nie L, Sun K, Ma W, Song D, Zheng L, Liang Z, Wu P, Yu F, Li J, Shan M, Zhao D, Li S, Kang B, Wu Z, Zhou Y, Liu K, Xiang Z, Ying J, Wang Z, Wu T, and Chen X 2022 *Nature* **604** 59
- [27] Li H, Zhao H, Ortiz B R, Oey Y, Wang Z, Wilson S D, and Zeljkovic I 2023 *Nat. Phys.* **19** 637
- [28] Chen H, Yang H, Hu B, Zhao Z, Yuan J, Xing Y, Qian G, Huang Z, Li G, Ye Y, Ma S, Ni S, Zhang H, Yin Q, Gong C, Tu Z, Lei H, Tan H, Zhou S, Shen C, Dong X, Yan B, Wang Z, and Gao H J 2021 *Nature* **599** 222
- [29] Deng H, Qin H, Liu G, Yang T, Fu R, Zhang Z, Wu X, Wang Z, Shi Y, Liu J, Liu H, Yan X Y, Song W, Xu X, Zhao Y, Yi M, Xu G, Hohmann H, Holbk S C, Drnagel

- M, Zhou S, Chang G, Yao Y, Wang Q, Guguchia Z, Neupert T, Thomale R, Fischer M H, and Yin J X 2024 *Nature* **632** 775
- [30] Yin J X, Lian B, and Hasan M Z 2022 *Nature* **612** 647
- [31] Jiang K, Wu T, Yin J X, Wang Z, Hasan M Z, Wilson S D, Chen X, and Hu J 2023 *Nat. Sci. Rev.* **10** nwac199
- [32] Wang Y, Wu H, McCandless G T, Chan J Y, and Ali M N 2023 *Nat. Rev. Phys.* **5** 635
- [33] Mi X R, Yang K Y, Gan Y H, Zhang L, Wang A F, Chai Y S, Zhou X Y, and He M Q 2023 *Tungsten* **5** 300
- [34] Wilson S D and Ortiz B R 2024 *Nat. Rev. Mater.* **9** 420
- [35] Zhou Y, Ye G, Luo S, Song Y, Lu X, and Yuan H 2024 *Supercond. Sci. Technol.* **37** 103001
- [36] Luo H, Gao Q, Liu H, Gu Y, Wu D, Yi C, Jia J, Wu S, Luo X, Xu Y, Zhao L, Wang Q, Mao H, Liu G, Zhu Z, Shi Y, Jiang K, Hu J, Xu Z, and Zhou X J 2022 *Nat. Commun.* **13** 273
- [37] Ortiz B R, Teicher S M, Kautzsch L, Sarte P M, Ratcliff N, Harter J, Ruff J P, Seshadri R, and Wilson S D 2021 *Phys. Rev. X* **11** 041030
- [38] Li H, Zhang T T, Yilmaz T, Pai Y Y, Marvinney C E, Said A, Yin Q W, Gong C S, Tu Z J, Vescovo E, Nelson C S, Moore R G, Murakami S, Lei H C, Lee H N, Lawrie B J, and Miao H 2021 *Phys. Rev. X* **11** 031050
- [39] Hu Y, Teicher S M, Ortiz B R, Luo Y, Peng S, Huai L, Ma J, Plumb N C, Wilson S D, He J, and Shi M 2022 *Sci. Bull.* **67** 495
- [40] Cho S, Ma H, Xia W, Yang Y, Liu Z, Huang Z, Jiang Z, Lu X, Liu J, Liu Z, Li J, Wang J, Liu Y, Jia J, Guo Y, Liu J, and Shen D 2021 *Phys. Rev. Lett.* **127** 236401
- [41] Nakayama K, Li Y, Kato T, Liu M, Wang Z, Takahashi T, Yao Y, and Sato T 2021 *Phys. Rev. B* **104** L161112
- [42] Zhao J, Wu W, Wang Y, and Yang S A 2021 *Phys. Rev. B* **103** L241117
- [43] Chapai R, Leroux M, Oliviero V, Vignolles D, Bruyant N, Smylie M P, Chung D Y, Kanatzidis M G, Kwok W K, Mitchell J F, and Welp U 2023 *Phys. Rev. Lett.* **130** 126401
- [44] Fu Y, Zhao N, Chen Z, Yin Q, Tu Z, Gong C, Xi C, Zhu X, Sun Y, Liu K, and Lei H 2021 *Phys. Rev. Lett.* **127** 207002
- [45] Yu F H, Wu T, Wang Z Y, Lei B, Zhuo W Z, Ying J J, and Chen X H 2021 *Phys. Rev. B* **104** L041103
- [46] Shrestha K, Chapai R, Pokharel B K, Miertschin D, Nguyen T, Zhou X, Chung D Y, Kanatzidis M G, Mitchell J F, Welp U, Popović D, Graf D E, Lorenz B, and Kwok W K 2022 *Phys. Rev. B* **105** 024508
- [47] Zhang D, Chen K W, Zheng G, Yu F, Shi M, Zhu Y, Chan A, Jenkins K, Ying J, Xiang Z, Chen X, and Li L 2024 *Nat. Commun.* **15** 6224
- [48] Lin X, Bridoux G, Gourgout A, Seyfarth G, Krämer S, Nardone M, Fauqué B, and Behnia K 2014 *Phys. Rev. Lett.* **112** 207002
- [49] Xiang Y, Li Q, Li Y, Xie W, Yang H, Wang Z, Yao Y, and Wen H H 2021 *Nat. Commun.* **12** 6727
- [50] Wang Z, Zhang W, Wang L, Poon T F, Tsang C W, Wang W, Xie J, Lam S T, Zhou X, Zhao Y, Wang S, Ai M Z, Lai K T, and Goh S K 2023 *Appl. Phys. Lett.* **123**
- [51] Tan H, Liu Y, Wang Z, and Yan B 2021 *Phys. Rev. Lett.* **127** 046401
- [52] Xu H S, Yan Y J, Yin R, Xia W, Fang S, Chen Z, Li Y, Yang W, Guo Y, and Feng D L 2021 *Phys. Rev. Lett.* **127** 187004
- [53] Lou R, Fedorov A, Yin Q, Kuibarov A, Tu Z, Gong C, Schvier E F, Büchner B, Lei H, and Borisenko S 2022 *Phys. Rev. Lett.* **128** 036402
- [54] Zhou X, Li Y, Fan X, Hao J, Dai Y, Wang Z, Yao Y, and Wen H H 2021 *Phys. Rev. B* **104** L041101
- [55] Li H, Zhang T T, Yilmaz T, Pai Y Y, Marvinney C E, Said A, Yin Q W, Gong C S, Tu Z J, Vescovo E, Nelson C S, Moore R G, Murakami S, Lei H C, Lee H N, Lawrie B J, and Miao H 2021 *Phys. Rev. X* **11** 031050
- [56] Liu G, Ma X, He K, Li Q, Tan H, Liu Y, Xu J, Tang W, Watanabe K, Taniguchi T, Gao L, Dai Y, Wen H H, Yan B, and Xi X 2022 *Nat. Commun.* **13** 3461
- [57] Xie Y, Li Y, Bourges P, Ivanov A, Ye Z, Yin J X, Hasan M Z, Luo A, Yao Y, Wang Z, Xu G, and Dai P 2022 *Phys. Rev. B* **105** L140501
- [58] Uykur E, Ortiz B R, Wilson S D, Dressel M, and Tsirlin A A 2022 *npj Quant. Mater.* **7** 16
- [59] Ratcliff N, Hallett L, Ortiz B R, Wilson S D, and Harter J W 2021 *Phys. Rev. Mater.* **5** L111801
- [60] Liu B, Kuang M Q, Luo Y, Li Y, Hu C, Liu J, Xiao Q, Zheng X, Huai L, Peng S, Wei Z, Shen J, Wang B, Miao Y, Sun X, Ou Z, Cui S, Sun Z, Hashimoto M, Lu D, Jozwiak C, Bostwick A, Rotenberg E, Moreschini L, Lanzara A, Wang Y, Peng Y, Yao Y, Wang Z, and He J 2023 *Phys. Rev. Lett.* **131** 026701
- [61] Kautzsch L, Ortiz B R, Mallayya K, Plumb J, Pokharel G, Ruff J P C, Islam Z, Kim E A, Seshadri R, and Wilson S D 2023 *Phys. Rev. Mater.* **7** 024806
- [62] Xiao Q, Lin Y, Li Q, Zheng X, Francoual S, Plueckthun C, Xia W, Qiu Q, Zhang S, Guo Y, Feng J, and Peng Y 2023 *Phys. Rev. Res.* **5** L012032
- [63] Stahl Q, Chen D, Ritschel T, Shekhar C, Sadrollahi E, Rahn M C, Ivashko O, Zimmermann M v, Felser C, and Geck J 2022 *Phys. Rev. B* **105** 195136
- [64] Ni S, Ma S, Zhang Y, Yuan J, Yang H, Lu Z, Wang N, Sun J, Zhao Z, Li D, Liu S, Zhang H, Chen H, Jin K, Cheng J, Yu L, Zhou F, Dong X, Hu J, Gao H J, and Zhao Z 2021 *Chin. Phys. Lett.* **38** 057403
- [65] Fukushima K, Obata K, Yamane S, Hu Y, Li Y, Yao Y, Wang Z, Maeno Y, and Yonezawa S 2024 *Nat. Commun.* **15** 2888
- [66] Liu Z, Shi Y, Jiang Q, Rosenberg E W, DeStefano J M, Liu J, Hu C, Zhao Y, Wang Z, Yao Y, Graf D, Dai P, Yang J, Xu X, and Chu J H 2024 *Phys. Rev. X* **14** 031015
- [67] Sur Y, Kim K T, Kim S, and Kim K H 2023 *Nat. Commun.* **14** 3899
- [68] Asaba T, Onishi A, Kageyama Y, Kiyosue T, Ohtsuka K, Suetsugu S, Kohsaka Y, Gaggl T, Kasahara Y, Murayama H, Hashimoto K, Tazai R, Kontani H, Ortiz B R, Wilson S D, Li Q, Wen H H, Shibauchi T, and Matsuda Y 2024 *Nat. Phys.* **20** 40
- [69] Guo C, Wagner G, Putzke C, Chen D, Wang K, Zhang L, Gutierrez-Amigo M, Errea I, Vergniory M G, Felser C, Fischer M H, Neupert T, and Moll P J W 2024 *Nat. Phys.* **20** 579
- [70] Frachet M, Wang L, Xia W, Guo Y, He M, Maraytta N, Heid R, Haghighirad A A, Merz M, Meingast C, and Hardy F 2024 *Phys. Rev. Lett.* **132** 186001
- [71] Miao H, Li H X, Meier W R, Huon A, Lee H N, Said A, Lei H C, Ortiz B R, Wilson S D, Yin J X, Hasan M Z, Wang Z, Tan H, and Yan B 2021 *Phys. Rev. B* **104** 195132
- [72] Park T, Ye M, and Balents L 2021 *Phys. Rev. B* **104**

- 035142
- [73] Ortiz B R, Gomes L C, Morey J R, Winiarski M, Borde-
lon M, Mangum J S, Oswald I W H, Rodriguez-Rivera
J A, Neilson J R, Wilson S D, Ertekin E, McQueen T M,
and Toberer E S 2019 *Phys. Rev. Mater.* **3** 094407
- [74] Xing Y, Bae S, Ritz E, Yang F, Birol T, Capa Salinas
A N, Ortiz B R, Wilson S D, Wang Z, Fernandes R M,
and Madhavan V 2024 *Nature* **631** 6066
- [75] Yang S Y, Wang Y, Ortiz B R, Liu D, Gayles J,
Derunova E, Gonzalez-Hernandez R, Šmejkal L, Chen
Y, Parkin S S, Wilson S D, Toberer E S, McQueen T,
and Ali M N 2020 *Sci. Adv.* **6** eabb6003
- [76] Haldane F D M 1988 *Phys. Rev. Lett.* **61** 2015
- [77] Varma C M 1997 *Phys. Rev. B* **55** 14554
- [78] Denner M M, Thomale R, and Neupert T 2021 *Phys.
Rev. Lett.* **127** 217601
- [79] Kenney E M, Ortiz B R, Wang C, Wilson S D, and Graf
M J 2021 *J. Phys. Condens. Mat.* **33** 235801
- [80] Saykin D R, Farhang C, Kountz E D, Chen D, Ortiz
B R, Shekhar C, Felser C, Wilson S D, Thomale R, Xia
J, and Kapitulnik A 2023 *Phys. Rev. Lett.* **131** 016901
- [81] Wang Y, Yang S Y, Sivakumar P K, Ortiz B R, Teicher
S M, Wu H, Srivastava A K, Garg C, Liu D, Parkin S S,
Toberer E S, McQueen T, Wilson S D, and Ali M N
2023 *Sci. Adv.* **9** eadg7269
- [82] Wang S, Feng X, Fang J Z, Peng J P, Sun Z T,
Yang J J, Liu J, Zhao J J, Wang J K, Liu X J,
Wu Z N, Sun S, Kang N, Wu X S, Zhensheng Z, Fu
X, Law K T, Lin B C, and Yu D 2024 *Preprint at
<https://arxiv.org/abs/2405.12592>*
- [83] Le T, Pan Z, Xu Z, Liu J, Wang J, Lou Z, Yang X,
Wang Z, Yao Y, Wu C, and Lin X 2024 *Nature* **630**
6469
- [84] Le T, Liu J, Wang Z, and Lin X 2024 *Chin. Phys. B* **33**
107402
- [85] Zheng L, Wu Z, Yang Y, Nie L, Shan M, Sun K, Song
D, Yu F, Li J, Zhao D, Li S, Kang B, Zhou Y, Liu K,
Xiang Z, Ying J, Wang Z, Wu T, and Chen X 2022
Nature **611** 682
- [86] Chen K Y, Wang N N, Yin Q W, Gu Y H, Jiang K, Tu
Z J, Gong C S, Uwatoko Y, Sun J P, Lei H C, Hu J P,
and Cheng J G 2021 *Phys. Rev. Lett.* **126** 247001
- [87] Zhao C, Wang L, Xia W, Yin Q, Deng H, Liu G, Liu J,
Zhang X, Ni J, Huang Y, Tu C, Tao Z, Tu Z, Gong C,
Wang Z, Lei H, Guo Y, Yang X, Yin J, and Li S 2024
Chin. Phys. Lett. **41** 127303
- [88] Guguchia Z, Mielke C, Das D, Gupta R, Yin J X, Liu
H, Yin Q, Christensen M H, Tu Z, Gong C, Shumiya N,
Hossain M S, Gamsakhurdashvili T, Elender M, Dai P,
Amato A, Shi Y, Lei H C, Fernandes R M, Hasan M Z,
Luetkens H, and Khasanov R 2023 *Nat. Commun.* **14**
153
- [89] Gupta R, Das D, Mielke III C H, Guguchia Z, Shiroka
T, Baines C, Bartkowiak M, Luetkens H, Khasanov R,
Yin Q, Tu Z, Gong C, and Lei H 2022 *npj Quant. Mater.*
7 49
- [90] Duan W, Nie Z, Luo S, Yu F, Ortiz B R, Yin L, Su H,
Du F, Wang A, Chen Y, Lu X, Ying J, Wilson S D,
Chen X, Song Y, and Yuan H 2021 *Sci. China Phys.
Mechan. Astron.* **64** 107462
- [91] Mu C, Yin Q, Tu Z, Gong C, Lei H, Li Z, and Luo J
2021 *Chin. Phys. Lett.* **38** 077402
- [92] Roppongi M, Ishihara K, Tanaka Y, Ogawa K, zda K,
Liu S, Mukasa K, Mizukami Y, Uwatoko Y, Grasset R,
Konczykowski M, Ortiz B R, Wilson S D, Hashimoto
K, and Shibauchi T 2023 *Nat. Commun.* **14** 667
- [93] Mine A, Zhong Y, Liu J, Suzuki T, Najafzadeh
S, Uchiyama T, Yin J X, Wu X, Shi X, Wang
Z, Yao Y, and Okazaki K 2024 *Preprint at
<https://arxiv.org/abs/2404.18472>*
- [94] Deng H, Liu G, Guguchia Z, Yang T, Liu J, Wang Z, Xie
Y, Shao S, Ma H, Lige W, Bourdarot F, Yan X Y, Qin
H, Mielke C, Khasanov R, Luetkens H, Wu X, Chang
G, Liu J, Christensen M H, Kreisel A, Andersen B M,
Huang W, Zhao Y, Bourges P, Yao Y, Dai P, and Yin
J X 2024 *Nat. Mater.* **23** 16391644
- [95] Zhang W, Liu X, Wang L, Tsang C W, Wang Z, Lam
S T, Wang W, Xie J, Zhou X, Zhao Y, Wang S, Tallon
J, Lai K T, and Goh G K 2023 *Nano Lett.* **23** 872
- [96] Deng H, Liu G, Guguchia Z, Yang T, Liu J, Wang Z, Xie
Y, Shao S, Ma H, Lige W, Bourdarot F, Yan X Y, Qin
H, Mielke C, Khasanov R, Luetkens H, Wu X, Chang
G, Liu J, Christensen M H, Kreisel A, Andersen B M,
Huang W, Zhao Y, Bourges P, Yao Y, Dai P, and Yin
J X 2023 *Nature* **617** 488
- [97] Holbæk S C, Christensen M H, Kreisel A, and Andersen
B M 2023 *Phys. Rev. B* **108** 144508
- [98] Ge J, Wang P, Xing Y, Yin Q, Wang A, Shen J, Lei H,
Wang Z, and Wang J 2024 *Phys. Rev. X* **14** 021025
- [99] Yang H, Ye Y, Zhao Z, Liu J, Yi X W, Zhang Y, Xiao
H, Shi J, You J Y, Huang Z, Wang B, Wang J, Guo H,
Lin X, Shen C, Zhou W, Chen H, Dong X, Su G, Wang
Z, and Gao H J 2024 *Nat. Commun.* **15** 9626
- [100] Liu Y, Liu Z Y, Bao J K, Yang P T, Ji L W, Liu J Y,
Xu C C, Yang W Z, Chai W L, Lu J Y, Liu C C, Wang
B S, Jiang H, Tao Q, Ren Z, Xu X F, Cao C, Xu Z A,
Zhou R, Cheng J G, and Cao G H 2024 *Nature* **632**
10321037